Macromolecular Coatings for Endotracheal Tubes Probed on An Ex Vivo Extubation Setup

Bernardo Miller Naranjo, Semai Naicker, and Oliver Lieleg*

Endotracheal intubation is indispensable in modern healthcare but typically entails two complications for the treated patients: biofouling-induced infections and friction-associated damage to the tissue. Coatings on the endotracheal tubes (ETT) may mitigate those problems, but they require a well-defined testing method to assess their functionality. Here, such a testing setup is presented, which allows for conducting ex vivo extubation experiments in a reproducible manner. With this setup, different coating strategies that immobilize porcine gastric mucins on the ETT surface are compared. The results demonstrate that covalent coatings generated from lab-purified mucins outperform the other variants in terms of their ability to decrease tissue damage, prevent lipid adsorption, and reduce cell attachment. With a similar approach as presented here, it should also be possible to evaluate macromolecular coatings generated on other medical tubing systems such as cardiac and urinary catheters and endoscopes.

1. Introduction

In many surgical interventions, endotracheal intubation is an indispensable procedure. However, there are numerous issues related to using endotracheal tubes (ETT). For instance, bacterial colonization of ETT surfaces and aspiration of pathogenic bacteria can lead to ventilator-associated pneumonia (VAP), which is one of the most common causes of infection among hospitalized patients requiring mechanical ventilation; and such complications lead to longer hospitalization as well as

B. Miller Naranjo, S. Naicker, O. Lieleg
TUM School of Engineering and Design
Department of Materials Engineering
Technical University of Munich
Boltzmannstraße 15, 85748 Garching, Germany
E-mail: oliver.lieleg@tum.de
B. Miller Naranjo, S. Naicker, O. Lieleg
Center for Protein Assemblies (CPA) and Munich Institute
of Biomedical Engineering (MIBE)
Technical University of Munich
Ernst-Otto-Fischer Straße 8, 85748 Garching, Germany

higher morbidity and mortality rates.[1–3] Other issues reported after intubation range from sore throats, coughing, and hoarseness to the presence of blood in the sputum – the latter of which is a clear indication of damage inflicted to the trachea tissue. And indeed, postprocedural bronchoscopy in extubated patients has proven that the tracheal mucosa is often injured as a consequence of the intubation procedure.[4]

To mitigate those problems, researchers have been trying to modify the interface between ETTs and the patient's trachea tissue by coating the ETT surface. For instance, Olson et. al added silver particles into hydrogel coatings on ETTs to reduce the bacterial burden, and they used dogs as a model system to evaluate the success of this strategy. In a different study, a dip-coating approach employing the antiseptic molecule silver-sulfadiazine was tested on ovine models; here, bacterial colonialization was successfully reduced on both, the ETT and the tissue.[5] In 2008, commercially available silver-coated tubes were tested in human patients; and, as intended, either a reduction or at least a delay in VAP occurrence was observed.[6] Other antimicrobial coatings introduced in the literature make use of ceragenin (which mimics antimicrobial growth inhibitors) or styrylbenzene.[7,8]

During intubation, the ETT surface is exposed to considerable shear forces, and this calls for strong bonds between the carrier material and the applied coating. However, many simple coating strategies cannot provide the required mechanical stability. In 2016, Yuk et al. covalently linked a hydrogel network to a substrate by means of surface silanization.[9] Yang et al. introduced a methodology to coat different substrates by gluing a dehydrated xerogel onto the surface of the material and then rehydrating the xerogel; such created coatings showed good resistance against shear forces.[10] Of course, good anti-bacterial properties and stability toward shear are not the only requirements for functional coatings on ETTs – improving the tribological properties of the ETT/tissue interface is equally desirable. Yet, this second aspect has received less attention so far. Approaches have been made using a combination of polymers and hyaluronic acid as coatings with good lubricating and anti-biofouling results and tissue damage was successfully reduced on animal models.[11–13] Very recently, Bai et al. presented a complex coating strategy that not only decreases friction in a technical setting using artificial materials as counterparts but also reduces the formation of tissue damage inflicted to trachea

**ADVANCED
SCIENCE NEWS**
www.advancedsciencenews.com

**ADVANCED
MATERIALS
INTERFACES**
www.advmatinterfaces.de

tissue as a consequence of in- and extubation.[14] However, a simpler approach that achieves similar results would be desirable to facilitate the application of such a coating in clinical practice.

In past work, macromolecular single-layer coatings generated from the glycoprotein mucin (the main structural and functional component of mucus) were shown to form very well-hydrated layers that can be firmly attached to a broad range of materials.[15–17] Such mucin coatings enable hydration lubrication (which is a key mechanism employed by mucus to reduce friction and wear in the human body and decrease friction and wear, both on artificial materials and tissues.[18–20] Moreover, such mucin-based coatings can considerably reduce the colonization of surfaces with bacteria.[21–27] Importantly, covalent mucin coatings have recently been demonstrated to withstand a range of harsh chemical conditions[16] as well as established sterilization methods,[28] which is why they might be a good choice to address both key problems arising from endotracheal intubation.

Here, we coat ETTs with mucins purified from porcine gastric mucus, and we assess how those coatings improve the tribological properties of ETT as well as their resistance to biofouling. To assess the former, we introduce a novel setup that allows us to conduct reproducible extubation tests with ex vivo trachea samples obtained from pigs. Our results show that covalent coatings generated from lab-purified mucins reduce the work required to conduct such an extubation process, suppress the transfer of tissue pieces onto the ETT surface, reduce the formation of stress-induced tissue damage, and provide the ETT surface with strong resistance toward lipid deposition and cell colonization.

2. Results and Discussion

For this study, a stretching setup introduced previously to measure the cohesion of bacterial biofilms is repurposed and modified such that it can perform controlled and reproducible extubation tests with porcine trachea samples.[29] As shown in **Figure 1**a, this device is assembled on a breadboard made from steel.

To determine the force needed to achieve a certain lateral movement, a force sensor is positioned between a linear motor and a shaft. The shaft is held by an air bearing (supplied with pressurized air adjusted to 70 psi) to keep the internal friction as low as possible. A custom-made adapter is connected to the distal side of the shaft to hold a hook, and this hook serves as an anchoring point to which the ETTs can be connected. A dedicated holder geometry (Figure 1b) keeps the porcine trachea sample in place by applying gentle pressure to the outside of the trachea; a resistive sensor is placed between the aluminum bottom piece of the trachea holder and the polydimethylsiloxane (PDMS) cushion to ensure that the applied pressure level is comparable between different experiments.

With this setup, the data acquisition is initiated automatically as soon as a force >0.1 N (which is above the noise level of the system) is detected by the sensor. An exemplary force curve obtained for a typical "extubation" experiment is shown in **Figure 2**a (phases I–IV). In detail, each measurement is
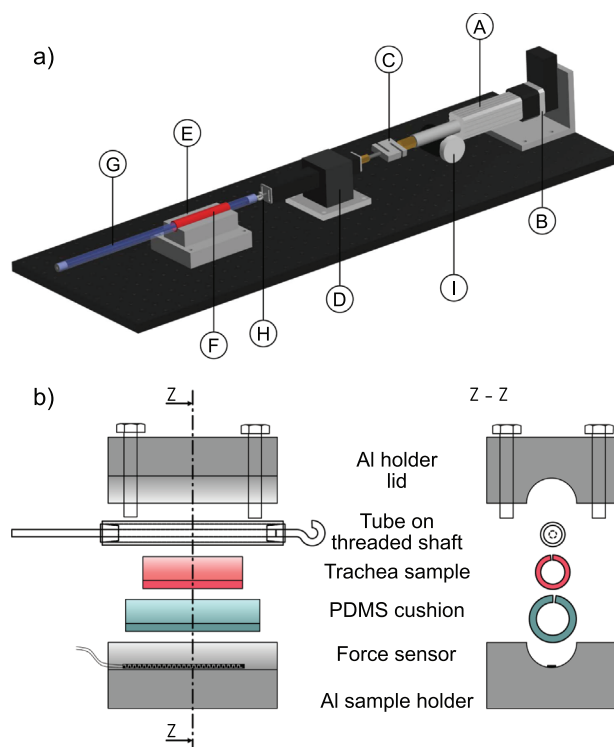

Figure 1. Computer aided design model of the setup used for conducting controlled extubation tests with ex vivo trachea samples. a) The device comprises a linear motor (A) with an integrated control unit (B), a force sensor (C), an air bearing (D), and a sample holder (E), which fixates a porcine trachea (F, colored in red). An ETT (G, colored in blue) is manually inserted into the trachea and connected to the moveable part of the air bearing via a hook (H); then, a controlled extubation procedure is conducted. A digital encoder (I) is used to measure the displacement of the shaft and to calculate the velocity at which the shaft is being driven in and out. b) Schematic illustration of the dedicated sample holder (E), which keeps a porcine trachea in place during an extubation test.

conducted as follows: An ETT and a porcine trachea sample are prepared and inserted into the sample holder as described in the experimental Section. Then, the motor references the "0" position, which produces a force signal >0.1 N and thus triggers automatic data acquisition. After referencing, the shaft is moved over a distance of 90 mm at a controlled speed of 15 mm s^{-1} until it reaches the loading position. This step is shown in phase I of Figure 2a; owing to the air bearing, the measured force remains at a very low level during this phase. In phase II, the motor keeps the shaft in this position for 4 s, which gives the user time to connect the ETT to the shaft. While the tube holder is manually connected to the motor shaft via a metallic ring, low forces (<1 N) are captured by the force sensor. Afterward, the motor pulls the shaft back (over the whole distance of 90 mm) at a constant speed of 15 mm s^{-1}, and this phase represents the actual "extubation" procedure (phase III): now, the ETT is pulled through the trachea and generates sliding friction during this process. Finally, in phase IV, the pulling process is terminated, and the force signal shows an exponential decrease, which can be attributed to a relaxation of the force sensor once the load is released. The force curve depicted in Figure 2a (phases I–IV) shows the mean and the
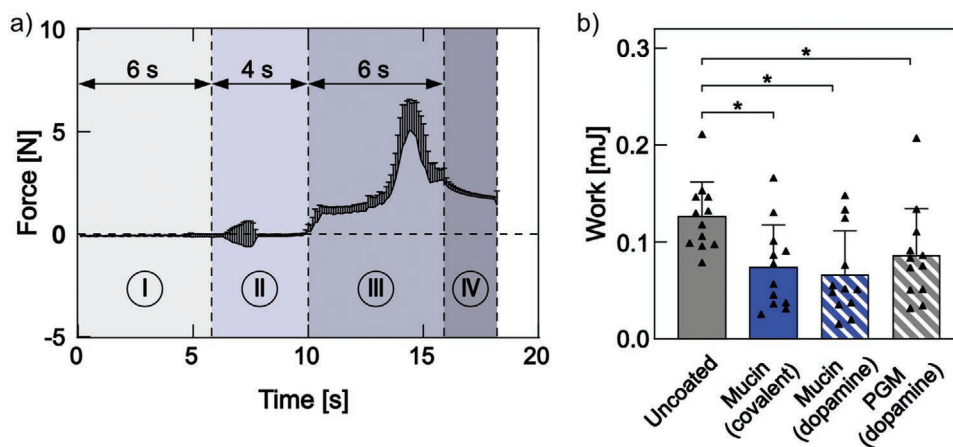
Figure 2. Typical force curve of an in vitro extubation process and the work required to conduct extubation of differently coated tubes. a) Graphical representation of the measured pulling force as a function of time as obtained for uncoated tubes during an extubation procedure. The curve shown represents the mean value of $n = 6$ independent tests; the error bars denote the standard deviation. b) Work calculated for the extubation process of tubes carrying different coatings; force curves as those shown in (a) were partially integrated, that is, for the time window representing phase III. The data shown depicts mean values as obtained from $n = 12$ independent samples; error bars denote the standard deviation. Asterisks mark statistically significant differences based on a p-value < 0.05.

positive standard deviation as calculated for six independent extubation experiments conducted with uncoated tubes. The reasonably small error bars show that those measurements are well repeatable.

By integrating the section of the force curve corresponding to phase III, we obtain the work necessary to pull a tube through the trachea at the conditions chosen here. An optical encoder was added to the setup to track the distance the shaft travels as a function of time. At a data acquisition rate of 10 points s^{-1}, this phase III of the force curve contains 60 data points which correspond to a total sliding distance of 90 mm. As shown in Figure 2b, this sliding process requires a mechanical work of (0.13 ± 0.03) mJ ($n = 12$) when uncoated tubes are used. In contrast, when using tubes carrying a covalently attached mucin coating (coating process represented in the Experimental Section and in Figure S1, Supporting Information), we measure a significant reduction in this value by ≈40%. In other words, the applied mucin coating is indeed able to facilitate the sliding process of the tube by reducing friction at the tube/trachea interface.

Given the improved sliding performance of the mucin-coated tubes, it is reasonable to assume that this mucin-coating has improved the surface properties of the tube such that it interacts better with the moist tissue. In fact, contact angle (CA) measurements show that the formerly hydrophobic tube material (CA ≈ 90°) is rendered hydrophilic by the coating (CA ≈ 60°, see **Figure 3**a). Whereas this reduction of the CA is not as strong as reported for mucin coatings conducted on other materials such as PDMS (the strength of alterations in the surface wetting properties achieved by a mucin coating depends strongly on the substrate material[16]), this result serves as a first indicator that the coating has successfully been generated on the ETT samples. Of course, an incomplete EDC/NHS-based coating could also provide lower CAs; thus, we next apply a periodic acid schiff (PAS) staining to verify the presence of mucins on the tube surface. And indeed, different from the uncoated tubes, the mucin-coated samples are intensively

stained in pink as typical for this PAS stain (Figure 3b,c). Further experiments conducted with fluorescently labeled mucins show that the mucin layer has a thickness of ≈3 μm (Figure S2, Supporting Information) and provides a smooth surface topography on the ETTs (Figure S3, Supporting Information). We conclude that the applied mucin coating renders the tube surfaces hydrophilic; moreover, we expect the attached mucins to enable hydration lubrication, which in turn might not only facilitate the sliding process of the tube but could also reduce the formation of surface damage on the treated tissue samples.

This notion is supported by a visual inspection of the tubes after the extubation procedure: On uncoated tubes, we find many spots carrying tissue material (those spots stain blue after incubation in a Trypan Blue (TB) solution, see **Figure 4**a); in contrast, the density of such tissue residues is much lower on mucin-coated tubes (Figure 4b). In other words, uncoated tubes generate sufficient tribological stress during the extubation process such that tissue pieces from the trachea are transferred onto the tube surface. Applying a mucin coating, however, can mitigate this effect.

In turn, this finding also suggests that the surface of the trachea tissue itself should have received damage as a consequence of the extubation process. A profilometric analysis of tribologically treated trachea samples seems to agree with this picture – but the (quite local) data obtained with this technique is by itself not strong enough to make a clear statement based on this optical assessment of the very smooth tissue alone (see Figure S4, Supporting Information). Thus, in the next step, we stain tribologically treated trachea tissue samples with the same staining solution, which we used to visualize tissue residues on the tubes. To assess the performance of the mucin coating regarding its ability to reduce tissue damage on the tracheal epithelia, we compare staining results obtained before and after the extubation experiment was conducted. With this approach, we can account for different initial levels of tissue damage present on the samples, which are a direct consequence of intrinsic sample-to-sample variations (as we work with ex vivo samples
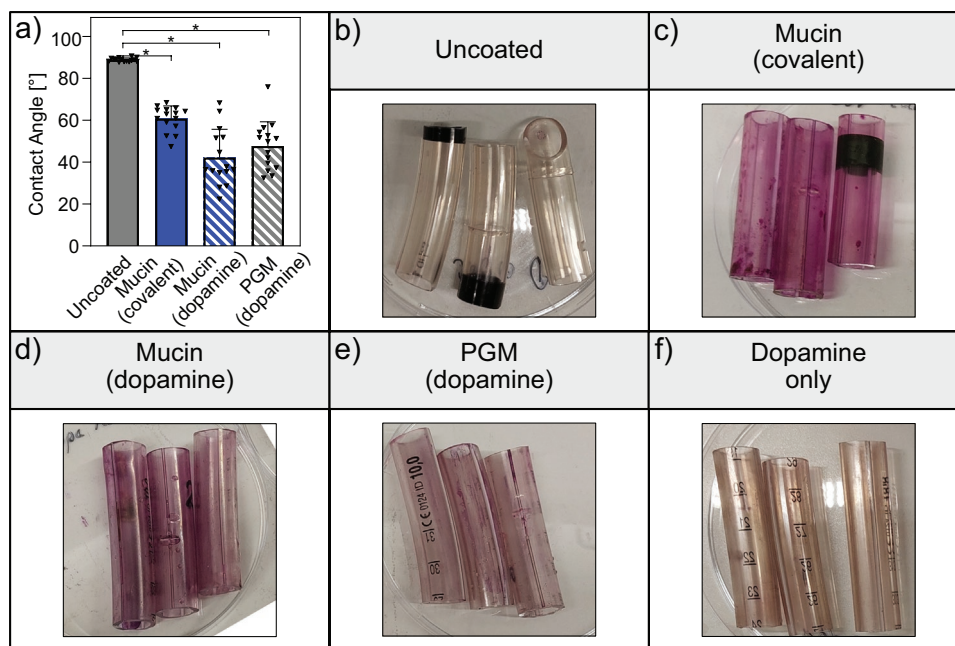
Figure 3. Visualization of mucins on the tube surface and wetting properties of the tubes. a) CA measurements conducted on the surface of differently coated tubes are compared to those obtained on uncoated tubes. The values shown depict mean values as calculated from 15 measurements conducted on three independently coated samples. Differences are considered to be statistically different based on a p-value <0.05 and marked with an asterisk. b–f) Results of a PAS staining that was applied to independently treated samples to test if mucins are successfully attached to the surface of the tubes. Three samples of ≈5 cm in length were tested for each condition: uncoated tubes, mucin-coated tubes (covalent and dopamine-assisted) and PGM-coated tubes (dopamine assisted). As a control group, tubes coated with dopamine only were tested as well.

obtained from a local butcher). And, as expected, we find that trachea samples stain more strongly after they were tribologically treated with an uncoated tube (Figure 4c,d). We here quantify this change in appearance of the obtained pictures with an algorithm, that calculates the difference in "blue dominance" as illustrated schematically in Figure 4e (see Experimental Section for details). When comparing the results obtained with this algorithm for trachea samples that were treated with uncoated and mucin-coated tubes, respectively, we find that the mucin coating leads to a significantly reduced increase in staining (Figure 4f). In other words, those coated tubes generate less damage on the trachea tissue than uncoated ones. Indeed, in several cases, the determined increase in tissue damage reported by the TB stain for samples treated with mucin-coated tubes is close to the value we find for trachea samples that were simply subjected to aging, that is, which were stored in the lab at comparable conditions as the tribologically treated ones without exposing them to sliding stress. Thus, we conclude that applying a covalent mucin coating to ETTs can reduce both, the number of tissue pieces/cell debris transferred onto the tube and the damage inflicted onto the trachea tissue.

In a final step, we ask whether the coating strategy used here to generate mucin layers on ETTs can be simplified without compromising the experimental outcome. In detail, we attempt a stepwise simplification: first, the covalent coating process is replaced by a dopamine-assisted coating procedure; this modification reduces the amount of tube treatment steps from six to two (see Experimental Section). Second, the lab-purified mucins are replaced with commercially available porcine gastric mucins (PGM). All three coating variants create smooth surfaces on the ETTs (Figure S3, Supporting Information), significantly reduce the work required to remove the tube from a trachea sample compared to uncoated tubes (Figure 2b), and convey hydrophilic properties to the initially hydrophobic tube surface (Figure 3a). However, when we subject such alternatively coated tube samples to a PAS staining to verify the presence of mucins, we observe weaker colorations than for the covalent coatings generated with lab-purified mucins (Figure 3d,e). If both, the coating procedure and the mucin type are altered, the intensity of the color reaction is the lowest. Control experiments with tubes that were coated with dopamine only (which appear brown instead of pink, which is the result of polydopamine formation on their surface as a side reaction of the dopamine incubation step, see Figure 3f) confirm that the pink coloration of our samples indeed originates from mucins. Thus, we conclude that dopamine-assisted coatings are less suitable in immobilizing mucins on the tube surface and that commercial mucins either interact less with dopamine layers than lab-purified mucins or are more difficult to stain with a PAS assay (and both issues may be due to the structural damages inflicted onto such commercial mucins during their industrial purification).[30] In addition to those differences in coating quality, we also find that the coating involving commercial porcine gastric mucins is less potent in preventing tissue damage on the trachea surface. In fact, for this particular coating type, we find similar levels of tissue damage as for uncoated tubes (Figure 4f). The dopamine-assisted coating employing lab-purified mucins, however, performs equally well in this particular aspect as the covalent coating making use of the same mucins (Figure 4f).
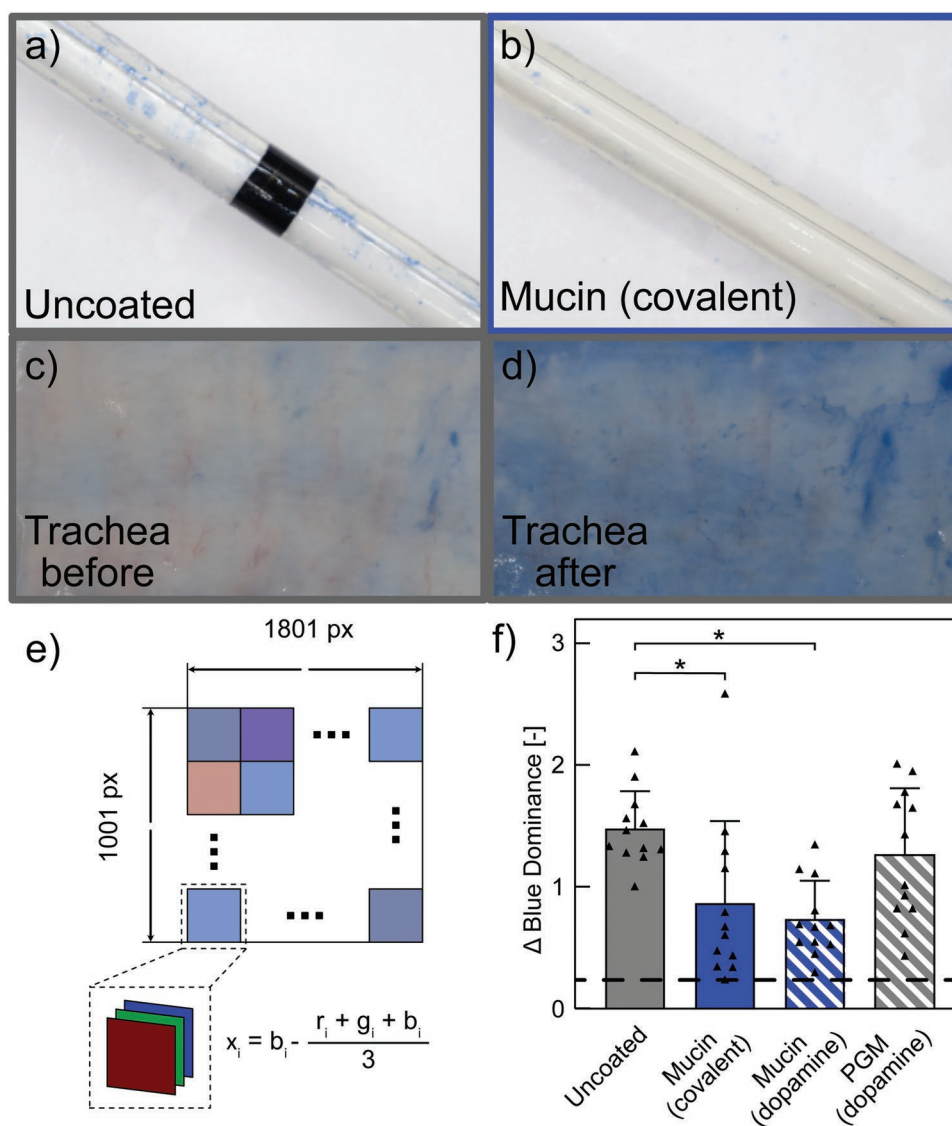
Figure 4. Tissue transfer to tubes and tissue damage caused on tracheal tissue after an extubation procedure. a) After being pulled through a porcine trachea, an uncoated tube is covered with many spots that indicate tissue fragments or cellular debris. b) On tubes carrying a covalent mucin coating, the density of such tissue/cell residues is much lower. Exemplary images of a TB-stained trachea sample before (c) and after (d) a completed extubation procedure using an uncoated tube. As a consequence of the applied tribological stress, the density of damaged cells on the tissue surface is increased, which results in a stronger blue signal from the TB stain. e) Quantification procedure to determine the increase in blue dominance (reporting on tissue damage) as obtained from images of stained trachea tissue samples after exposing them to an extubation procedure (see Experimental Section). f) Comparison of surface damage afflicted to porcine trachea samples after an extubation process conducted with differently coated tubes. The dotted grey line shows the increase in blue dominance obtained from images of a control group, where tissue samples were subjected to the full treatment procedure without exposing them to tribological load. Error bars represent the standard deviation as calculated from $n = 12$ independent samples. Asterisks mark statistically significant differences based on a p-value of $p < 0.05$.

In the last step of this study, we ask how the three different mucin coatings discussed above perform with regard to reducing biofouling, that is, if they can reduce the undesired adsorption of molecules and cells onto the tube surface (see **Figure 5**a and b). We expect this question to be directly related to the tribological performance of the coatings as an alteration of the surface properties of the mucin-coated tubes by the deposition of biological material will interfere with the function of the coating – and incomplete coatings (as indicated by the weaker staining results shown in Figure 3) will be more prone

to such an issue. In the context of tracheal tissue surfaces, the surfactant dipalmitoylphosphatidylcholine (DPPC) is a highly relevant molecule.[31–33] Owing to its amphiphilic nature, this phospholipid should readily adsorb to the rather hydrophobic surface of the commercial PVC tubes used here. And indeed, when uncoated tube pieces are incubated in a DPPC solution for 30 min, the initially transparent tube pieces turn opaque (Figure 5a), which indicates strong lipid deposition. In contrast, tube pieces carrying a covalent mucin coating remain virtually pristine after exposure to those lipids (Figure 5c). This
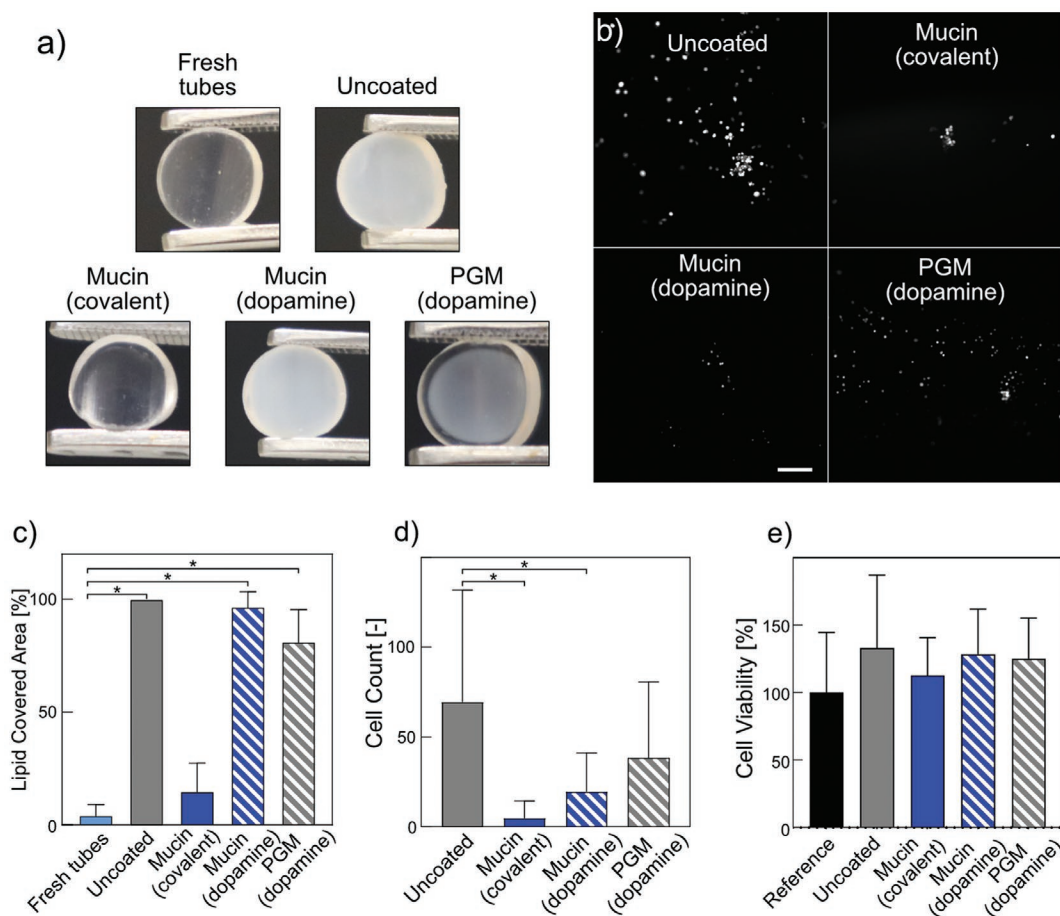
Figure 5. Anti-biofouling properties of different mucin-based coatings. a) Images of different tube samples after incubation in a DPPC solution. b) Colonization of different tube samples by epithelial cells as visualized by microscope images of fluorescently stained cells. The scale bar represents 200 μm and applies to all images shown in (b). c) Quantification of the images obtained in the lipid deposition test shown in (a). d) Quantification of microscopy images such as those shown in (b). e) Cell viability tests conducted with HeLa cells to assess the biocompatibility of the different coatings. Data shown in (c–e) depict the average; error bars denote the standard deviation. The sample size was $n = 5$ for the lipid tests and a total of 20 images were acquired from $n = 5$ samples for the cell colonization tests. The sample size for the cell viability tests was $n = 8$. Asterisks mark statistically significant differences based on a p-value of $p < 0.05$.

underscores the high potential of such mucin coatings for applications where the material gets in contact with lipid-rich lung tissue. Interestingly, the two other two mucin-coatings (dopamine-based, PGM-based) fail in creating such strong lipid-repelling properties on the tube material.

Of course, when inserted into a trachea, ETTs do not only come into contact with lipids but also with epithelial cells. To test if the mucin coatings generated here can also suppress the adhesion of such epithelial cells to the tube surface, we conduct colonization tests using HeLa cells as a model cell line. As shown in Figure 5b and d, the covalent mucin coating has a strong cell-repelling effect, and this agrees with previous findings obtained with mucin coatings on different substrates. A significant reduction in the number of adherent cells is also observed for dopamine-assisted mucin coatings, but not for coatings generated from commercial PGMs. Those findings suggest that the ability of the mucin coatings to reduce tissue damage is – at least in part – related to their capacity to mitigate biofouling events such as lipid deposition and cell

adhesion. Our results also agree with previous studies on the anti-biofouling properties of mucins, where it was shown that the glycosylation pattern along the polypeptide backbone of the mucins needs to be intact to achieve good results.[15,27] Thus, defective commercial PGMs[30] may render the material hydrophilic, but can only provide inferior anti-biofouling properties. To test for putative cytotoxic effects of the different coatings, a cytocompatibility test was performed according to ISO 10 993. As shown in Figure 5e, none of the generated coatings compromised the viability of the epithelial cells (HeLa) selected for those tests.

For the past decades, many materials have been tested as options to fabricate ETTs from, and many positive results have been reported.[2,34,35] Nevertheless, the friction and tissue damage generated at the interface between ETTs and human tissue has been largely neglected. In fact, the (to our knowledge) first attempt to measure the force required to extubate a patient was reported by Carlson et. al. in 2007.[36] Here, however, only the peak force occurring during the extubation process

was considered; moreover, the extubation was performed manually (as typical for clinical practice), which makes it difficult to reproduce those tests. In contrast, with the technical setup presented here, well-reproducible extubation tests can be conducted, in which the pulling velocity and the normal pressure acting between the ETT and the trachea tissue can be controlled. This setup employs materials and geometries relevant for the clinical application and is sensitive enough to allow for comparing different ETT surface modifications – without the need to use living animal models.

Still, also the method introduced here comes with its limitations. For instance, the pressure applied to the interface between the ETT and the tracheal tissue is kept constant during the extubation process; this does not fully recreate the situation found in vivo, where the tip of the ETT creates a pressure peak on selected regions of the trachea. Moreover, another source of damage to the tissue might be the ETT cuff, which is inflated to hold the tube in place and seals the lumen of the trachea during a medical intervention. In the experiments conducted here, this cuff was removed, which simplifies the ETT geometry. Another simplification of the tests conducted is the short time span during which the ETTs are in contact with the tracheal tissue ($\approx$1 min). When a patient is intubated, the tube remains in the patient's body for several hours – or even for several days. It is likely that, for such longer contact times (where the level of biofouling can be much higher than what we can recreate here), the advantages brought about by a mucin coating would be even more pronounced. Nevertheless, even with the short contact times used in this study, the advantage brought about by applying a mucin coating to the ETTs was significant, and clear differences between the different coating variants could be determined.

Of course, in a real clinical scenario, the intubation process can contribute to the formation of tissue damage as well; however, for technical reasons, implementing a controlled insertion process of an ETT into tracheal tissue is very challenging. However, with major modifications, the setup presented here has the potential to study the process of intubation as well. For instance, it would be necessary to guarantee a perfectly parallel alignment of the trachea sample and the ETT (to ensure that the normal pressure acting on the tissue is reproducible). In addition, the tube sample needs to be inserted precisely into the middle of the trachea sample – and this requires a more refined control over the straightened tube geometry than achieved here. With such modifications, it should then be possible to evaluate the mechanical stability of a mucin coating (or a coating generated from other macromolecules) as well as the formation/prevention of tissue damage over a full intubation/extubation cycle.

3. Conclusion

In conclusion, we here present a novel setup for conducting controlled extubation experiments with porcine trachea samples. This setup allows us to compare different mucin-based coatings that render the ETT surface hydrophilic, and we find clear differences in the wear-reducing and anti-biofouling abilities of the different coatings investigated here. Thus, our approach may serve as an ex vivo/in vitro platform for further developments in the field of biomedical engineering: it is easily possible to test a broad range of different coatings and tube materials without the economic, bureaucratic, and ethical issues related to animal tests. Moreover, the approach presented here does not have to be limited to testing ETTs, but can also be modified to probe other devices that create shear stress on tissues when they are introduced into the body, for example, urinary or cardiac catheters. Furthermore, the anti-biofouling, wear-reducing mucin coatings studied here may also be highly valuable for other medical devices such as implants and pacemakers.

4. Experimental Section

Statistical Analysis: All data sets were tested regarding statistically significant differences. To test for normal data distribution, a Lilliefors test was used; to test for equal variances, a two-sample F-test was employed. In case of normal data distribution and equal variances, a two-sample t-test was used to test for statistically significant differences between data sets. For data sets with normal distribution and non-equal variances, a Welch's t-test was employed. For data with no normal distribution, a Wilcoxon-Mann-Whitney test was employed. All statistical analyses were conducted using the software Matlab (version 2022a, Mathworks, MA, USA). Differences were considered to be statistically different if a p-value lower than 0.05 was obtained.

Mucin Purification: Porcine gastric mucin was purified as described by Marcynski et al. (2022). In brief, gastric mucus was harvested from porcine stomachs that were purchased at a local slaughterhouse on the day of processing. The pig stomachs were cut open and gently rinsed with tap water. Then, mucus was collected by manually scraping the inner surface of the tissue. The obtained mucus was diluted 5-fold in 10 mM sodium phosphate-buffered saline (PBS, pH 7.0) enriched with 170 mM NaCl and 0.04% (w/v) sodium azide, and stirred at 4 °C overnight. The homogenized mucus was subjected to four consecutive filtering steps by passing the mucus through metal grids with mesh sizes of 1 mm, 500, 200, and 125 µm, respectively. Afterward, the mucin glycoproteins were isolated from the other mucus constituents by size exclusion chromatography (SEC) using an ÄKTA purifier system (GE Healthcare, Munich, Germany) equipped with an XK50/100 column packed with Sepharose 6FF resin (GE Healthcare). The collected mucin fractions were pooled and the NaCl concentration was increased to 1 M. Then, this mucin solution was dialyzed against ultrapure water and concentrated by cross-flow filtration (MWCO: 100 kDa; QuixStand benchtop crossflow system, GE Healthcare) equipped with a hollow fiber module with a molecular weight cut-off of 100 kDa (Xampler Ultrafiltration Cartridge, GE Healthcare). Finally, the concentrate was lyophilized and stored at −80 °C until further use. Commercial porcine gastric mucins (PGM type II) were obtained from Sigma–Aldrich and used as is.

Covalent Coating: Commercial ETTs were purchased from Radecker Notfallmedizin (Ammerbuch/Entringen, Germany).

Lab-purified porcine gastric mucins were covalently bound to the outer surface of endotracheal intubation tubes using a procedure described in Winkeljann et al (see Figure S1, Supporting Information).[19] In brief, the PVC tubes were removed from their sterile packaging and carefully cut into pieces of $\approx$15 cm in length. After rinsing in 80% (v/v) ethanol and ultrapure water, the tubes were plasma-activated in a plasma oven (SmartPlasma 2.0, plasma technology GmbH, Herrenberg-Gültstein, Germany) using atmospheric plasma at a pressure of 0.4 mbar and an intensity of 30 W for 90 s. In this step, the methyl groups of the surface were substituted with hydroxyl groups. Then, the coupling agent N-[(3-trimethoxysilyl)propyl]-ethylenediamine triacetic acid trisodium (TMS-EDTA, abcr GmbH, Karlsruhe, Germany) was used to prepare the sample surface for the following carbodiimide coupling steps. TMS-EDTA was

**ADVANCED
SCIENCE NEWS**

www.advancedsciencenews.com

**ADVANCED
MATERIALS
INTERFACES**

www.advmatinterfaces.de

diluted to a concentration of 1% (v/v) in 10 mM acetate buffer (pH 4.5), and the samples were incubated in this solution for 5 h at 60 °C. After this step, the samples were dipped into isopropanol (>99.5% (v/v)) and washed in 96% (v/v) ethanol for 1 h on a rolling shaker (70 rpm, RS-TR 05, Phoenix Instrument GmbH, Garbsen, Germany). Then, the samples were incubated at 110 °C to stabilize the siloxane bond. Afterward, the ETTs were incubated on a rolling shaker (70 rpm) where they were immersed in 100 mM MES buffer (pH 5.0) containing 5 mM EDC and 5 mM sulfo-NHS at room temperature for 30 min. In a final step, mucins were dissolved in 1x Dulbecco's phosphate-buffered saline (DPBS; Lonza, Verviers, Belgium) in a concentration of 0.1% (w/v), and the tubes were incubated in the mucin solution at 4 °C for 12 h. Finally, the coated tubes were gently washed in 80% (v/v) ethanol and stored in 20 mM HEPES (4-(2-hydroxyethyl)-1-piperazine ethane-sulfonic acid) buffer (pH 7) until further use.

Dopamine-Assisted Coating: As a non-covalent alternative, a two-step coating process was employed that takes advantage of the intrinsic stickiness of dopamine to create a mediating layer on the tubes that allows the mucins to attach spontaneously. To do so, the tubes were removed from the sterile packaging and cut into pieces of ≈15 cm in length that were subsequently rinsed in 80% ethanol and Millipore water. Then, the tubes were first incubated in 50 mM tris(hydroxymethyl) amino-methane (Tris) buffer (pH 8.5) containing 0.4% (w/v) dopamine for 2 h. Then, the tubes were transferred into a HEPES solution (20 mM; pH 7.0) containing 0.1% (w/v) of either lab-purified mucins (see above) or commercially available porcine gastric mucins (Type II, Sigma-Aldrich, St. Louis, MO, USA) and incubated for 1 h. Finally, the tubes were rinsed with 80% (v/v) ethanol and Millipore water and incubated in HEPES buffer until further use.

Periodic Acid Schiff (PAS) Staining: To verify the presence of mucins on the surface of the coated tubes, a PAS staining was conducted. For this purpose, tube samples of 5 cm in length were prepared and three such samples were coated independently for each coating variant: uncoated (control group), covalent mucin coating, dopamine-assisted mucin coating, and dopamine-assisted PGM coating. Additionally, three samples were coated with dopamine only to test whether the PAS stain would also react to dopamine (which could affect the interpretation of the results). The samples were then dipped into a 0.5% (v/v) solution of periodic acid for 5 min and afterward incubated in a Schiff reagent solution for 15 min. Finally, pictures of the stained tubes were acquired with a digital system camera (Canon EOS M50 Mark II, Canon Inc., Tokyo, Japan).

Contact Angle Measurements: To compare the wetting behavior of coated and uncoated ETTs, CAs were determined on 5 cm long tube pieces cut from the ETTs. A commercial drop-shape analyzer device (DSA25S, Krüss GmbH, Hamburg, Germany) was used to perform these measurements. Uncoated samples were washed with 70% (v/v) ethanol and rinsed with Millipore water; coated samples were removed from the storage buffer (see above). Prior to conducting measurements, all samples were dried for ≈3 s using oil-free pressurized air (Aero Duster 105/2). A 2 µL droplet of ultrapure water was placed onto each sample (which was placed with its long axis perpendicular to the light path), and lateral images were captured with a high-resolution built-in camera (acA1920, Basler, Ahrensburg, Germany).

Preparing Tracheal Tissue: Fresh porcine trachea samples were obtained from a local butcher. Adjacent tissue was carefully removed, and special care was taken not to damage the inner walls of the tracheas. Then, the trachea samples were rinsed in 1x Dulbecco's PBS (DPBS) to remove residual mucus. This step was introduced to reduce sample-to-sample variations (as it was noticed that the amount of mucus present on the inner surface of the tracheas varied strongly between samples). Afterward, the tracheas were slit open longitudinally and two test pieces (5 cm in length and 4 cm in width) were cut from each sample.

Preparing Endotracheal Tubes: Commercial ETTs were quite stiff and possessed an intrinsic curvature along the longitudinal axis. Thus, to straighten the tubes so a controlled and reproducible sliding process was possible in the linear setup developed here, a threaded shaft (M4 thread) was inserted into the tube and kept in place by two metallic plugs with M4 threads (Figure 1). At one side of the construct, the M4 threaded end was connected to a hook, which allowed for connecting the tube to the motor of the pulling device.

Those straightened tubes were then inserted into a freshly prepared trachea sample that was slit open along its long axis. This procedure ensured that inserting the tubes into the trachea leaves most of the tissue surface undisturbed, which was crucial for the tissue damage evaluation that aimed to conduct after having performed a controlled extubation test. The trachea sample, in turn, was placed into a tailor-made PDMS cushion, below which a force sensor was placed. Then, the whole construct was clamped between two aluminum pieces, which were connected to each other via screws. Here, a force sensor (ZD10-100, Walfront Electronics, Shenzhen, People's Republic of China) was placed between the PDMS cushion and the lower half of the aluminum casing, which allowed to close the sample holder in such a way, that different tube/trachea samples experienced similar pressure levels of ≈16 kPa.

Technical Components of the Extubation Setup: Here, an existing device initially designed to conduct lateral stretching tests with bacterial biofilms was repurposed and modified such that it could perform controlled extubation tests using commercial ETTs and porcine trachea samples. In particular, the modified device was supposed to conduct a well-controlled pulling procedure that removes the tube from the trachea at a constant speed while recording the forces occurring during this process. In the following, it was listed that the technical components of this setup together with important specifications of those components.

To pull the tube through the trachea, a Colibri-L LE17 linear stage (GUNDA Electronic GmbH, Friedrichshafen, Germany) was employed. This linear stage has a precision of ≈1 µm and can travel at speeds of up to 300 mm s^{-1}. It has an integrated control unit, which allows the motion protocol to be saved on the EEPROM (Electrically Erasable Programmable Read-Only-Memory). This integrated control unit was programmed using the software Colibri BAC Konfiguration (Gunda Electronic GmbH, Schlier-Wetzisreute, Germany).

An air bearing (IBS Precision Engineering, Eindhoven, The Netherlands) was used to reduce the internal friction of the system occurring during lateral movement. As a thin air film builds up between the static and the moving parts of the device, stick-slip events were suppressed and the internal friction of the device was decoupled from friction forces occurring between the tube sample and the trachea. This air bearing was supplied with pressurized air, which was filtered and dried using standard oil removal and filter components (Parker Hannifin Manufacturing Limited, Gateshead, United Kingdom). The filtered air flowed through the case of the bearing, which contained a porous material. A pressure relief valve was used to adjust the air supply at a pressure ≈70 psi. In the center of the case, a shaft with a rectangular cross section rested on an air cushion, that allowed the shaft to move horizontally with almost no friction. With this air bearing, the maximal amplitude of lateral motion was ≈100 mm.

The movable shaft of the air bearing was connected to an S-shaped force sensor (KD-40s 20N, ME-Meßsysteme GmbH, Hennigsdorf, Germany). Pilot tests were conducted using a force sensor with a maximum loading force of 200 N; however, all those preliminary measurements returned force values below 20 N, which allowed to switch to a sensor with a lower maximum loading force of 20 N (which improves the resolution of the recorded force values). This force sensor was connected to a 24-Bit amplifier (GSV-2, ME-Meßsysteme GmbH, Hennigsdorf, Germany), which in turn was connected via USB to a Windows PC for data acquisition. With this sensor configuration, a force resolution in the range of 2 mN was obtained.

An optical encoder (model LPD3806, Fockety, People's Republic of China) was used to measure the distance traveled by the motor shaft. A custom-made PTFE adapter was used to connect the encoder to the motor shaft such, that the linear movement of the motor shaft was transferred into a rotational movement of the encoder, which was clamped onto the breadboard. The signal from the optical encoder was processed using an Arduino Board (Arduino UNO R3, Somerville, MA, United States of America).

Detecting Surface Alterations on Trachea Tissue Samples: First, the trachea samples were prepared as described in section 2.1; then, they were incubated for 40 min in a 0.01% (v/v) TB solution (Trypan Blue solution, Sigma Aldrich, Burlington, MA, USA) prepared in 1x DPBS. Next, the samples were washed in DPBS for 20 s, and images of the stained trachea samples were acquired using a digital system camera (Canon EOS M50 Mark II, Canon Inc., Tokyo, Japan) at a defined distance (see below). This step allowed us to assess the initial state of the sample prior to conducting the extubation experiment as it quantified pre-existing tissue lesions before the samples were exposed to tribological stress (this helped to account for sample-to-sample variations).

Quantifying Tissue Damage Based on Tissue Stainings: On a macroscopic level, the tissue damage caused by the extubation procedure was quantified by analyzing the tissue coloration after incubation in a TB dye solution (see above). This dye was taken up by cells if their membrane was damaged; this approach was used previously to assess tissue damage in combination with image analysis.[37–39] As all trachea samples analyzed here were incubated in the TB solution before and after the extubation experiments, the damage generated by the extubation process could be quantified by comparing the portion of the sample that became colored after the tribological stress was applied. To guarantee identical illumination conditions throughout all experiments, images were taken inside a photo cube of 40 cm × 40 cm × 40 cm (Caruba, Bathoorn, Sweden) set to maximum light intensity. Pictures were acquired using a digital camera (Canon EOS M50 Mark II) with an aperture value of F6.3, a shutter speed of 1/125, and an ISO speed of ISO100. A tripod was used to establish a constant distance of ≈35 cm between the samples and the camera.

The images obtained for the different samples were then analyzed using the software MATLAB R2022a (Mathworks Inc., Massachusetts, USA). With the raw2rgb function, the RGB values of each pixel (r_i, g_i, b_i) were extracted and saved in a 1001-by-1801-by-3 matrix. Then, these values were transformed from an unsigned integer format uint16 to double. For each pixel, the dominance of blue color was calculated according to equation 1 (see Figure 4e for a schematic representation of this process):

$$x_i = b_i - \frac{r_i + g_i + b_i}{3} \tag{1}$$

Conducting this calculation for all i pixels in the image and averaging the resulting values x_i returns a number that quantifies the dominance of blue color in a given image (in such a case, the result is larger than zero; for a grey pixel, the RGB values are all identical, so $x_i = 0$ for such pixels). In addition, this method comes with the advantage that it allows to automatically filter out artifacts produced by the reflection of white light on the humid surface of the tracheas.

Lipid Adsorption Tests: The anti-biofouling properties of the different coatings were investigated via lipid deposition tests. Dipalmitoylphosphatidylcholine (DPPC, Avanti Polar Lipids, AL, United States of America) was used as a model of the lung surfactant, and an aqueous solution containing 0.05% (w/v) DPPC and 2.5% (w/v) tetrahydrofurane (Sigma-Aldrich, St. Louis, MO, USA) were prepared in cooled Millipore water (6–10 °C). Cylindrical samples with a diameter of 7 mm were stamped from freshly unpacked ETTs and subsequently coated according to the different strategies discussed in section 4.2.

Then, the ETT samples were first dipped into Millipore water for 20 s and then placed into a vial containing the DPPC solution. After exposure to the lipid solution for 60 min, the samples were again washed in Millipore water for 10 s. Afterward, images of the samples were obtained on a black background using a digital system camera (Canon) and analyzed using the software ImageJ2 (version 2.3.0/1.53q, 2021).

For this image analysis, the area of interest was first manually marked by following the contour without the border (to avoid a falsification of data due to reflection effects). The images were then converted into 32-bit grayscale, and a threshold filter (high-pass; threshold value: 150) was implemented to assess the segments covered with lipids. Finally, the area covered with lipids was compared to the area of the whole sample.

In Vitro Cell Colonization Tests: To assess the ability of the different coatings to reduce surface colonization by eukaryotic cells, the established epithelial cell line HeLa was selected. Cylindrical PVC samples were stamped out of freshly unpacked ETTs (see 4.8) and then coated as described above. After coating, the samples were dipped into 96% (v/v) ethanol and then placed into wells of an 8-well plate (µ-Slide ibidiTreat plate, ibidi GmbH, Gräfelfing, Germany) with their concave side facing up. HeLa cells were cultivated in standard medium (DMEM supplemented with 5% FCS and 1% penicillin/streptomycin) at 37 °C and 5% CO2. 50000 cells were seeded onto each sample and incubated for 4 h at 37 °C. Afterward, the samples were then gently rinsed with sterile DPBS, and the remaining cells were stained with 50 µL of a live/dead solution (1×10^{-6} M calcein-AM, 2×10^{-6} M ethidium homodimer-1, Invitrogen, Carlsbad, CA, USA) for 30 min. Subsequently, fluorescence images were acquired using a fluorescence microscope (DMi8, Leica, Wetzlar, Germany) equipped with an FITC filter cube (Ex = 460–500, DC = 505, Em = 512–542, Leica). Exposure times were first optimized and then applied to all images.

For each condition (uncoated, mucin/covalent, mucin/dopamine, and PGM/dopamine), five independent samples were prepared, and four images were acquired from each sample. In the acquired images, the cells were counted manually.

Cytotoxicity Tests: To study the biocompatibility of the different coatings, a leaching test according to the norm ISO 10 993 was conducted. In brief, ETT samples of ≈1 cm in length were prepared for the different conditions presented in this work: Uncoated, covalent mucin coating ("Mucin (covalent)"), dopamine-mediated mucin coating ("Mucin (dopamine)") and dopamine-mediated coating using commercial mucin ("PGM (dopamine)"). After coating, all samples were first rinsed with an 80% (w/v) ethanol solution and then exposed to UV light for 30 min (BLX-254, Vilber Lourmat GmbH, Eberhardzell, Germany). Afterward, the samples were placed into 5 mL of the sterile medium used for the cell tests described in section 4.9 (i.e., DMEM supplemented with 5% FCS and 1% penicillin/streptomycin) and incubated for 24 h at 37 °C and 5% (v/v) CO₂.

HeLa cells were seeded from frozen stock and maintained in the cell medium at 37 °C and 5% CO₂ until confluency was reached. Then, 5000 cells were transferred into wells containing 100 µL of fresh medium. A total of eight wells were prepared for each of the following groups: Uncoated, Mucin (covalent), Mucin (dopamine), PGM (dopamine), and untreated. The last group served as another control, that is, it contained cells exposed to a standard cell medium which was not incubated with an ETT sample ("reference").

After 24 h of incubation, 50 µL of medium was removed from each well containing the cells and replaced with 50 µL of a "leaching" medium (i.e., a media sample, in which one of the differently coated ETT samples had been incubated for 24 h). Then, the cells were incubated for 24 h and the cell viability was determined. For this purpose, the medium was carefully withdrawn from the wells containing the cells. 150 µL of a 2% (v/v) water-soluble tetrazolium salt (WST, WST-1, Roche Diagnostics GmbH, Mannheim, Germany) solution prepared in cell medium was pipetted into each well. In addition, 8 fresh wells were filled with 150 µL of this WST solution to serve as a blank for the following measurements.

After 1 h of incubation, the absorbance of those WST solutions was quantified with a plate reader (SpectraMax ABS Plus, Molecular Devices LLC, CA, USA). The obtained values were treated as follows: The average absorbance was calculated for the 8 wells containing a WST solution only. This average was subtracted from all measurements conducted for wells containing cells. Then, the mean absorbance was calculated for the "reference" and this value was used to normalize the absorbance measured for the other four groups.

Supporting Information

Supporting Information is available from the Wiley Online Library or from the author.

Acknowledgements

Conflict of Interest

The authors declare no conflict of interest.

Author Contributions

O.L. and B.M.N. designed the study. B.M.N. and S.N. conducted the experiments, and B.M.N. analyzed data. The manuscript was written by B.M.N. and O.L.

Data Availability Statement

The data that support the findings of this study are available from the corresponding author upon reasonable request.

Keywords

biofouling, glycoprotein, mucin, surface modification, tissue damage

[1] M. E. Olson, B. G. Harmon, M. H. Kollef, *Chest* **2002**, *121*, 863.
[2] C. F. Haas, R. M. Eakin, M. A. Konkle, R. Blank, *Respir. care* **2014**, *59*, 933.
[3] J. Thomas, L. Corum, K. Miller, in *The role of biofilms in device-related infections*, Springer, Berlin, Heidelberg **2008**. pp. 75–107.
[4] L. Liu, W. Wu, X. Tuo, W. Geng, J. Zhao, J. Wei, X. Yan, W. Yang, L. Li, F. Chen, *Artif. Organs* **2010**, *34*, 426.
[5] L. Berra, L. D. Marchi, Z.-X. Yu, P. Laquerriere, A. Baccarelli, T. Kolobow, *Anesthesiology* **2004**, *100*, 1446.
[6] M. H. Kollef, *JAMA.* **2008**, *300*, 805.
[7] M. M. Hashemi, J. Rovig, J. Bateman, B. S. Holden, T. Modelzelewski, I. Gueorguieva, M. Von Dyck, R. Bracken, C. Genberg, S. Deng, P. B. Savage, *J. Antimicrob. Chemother.* **2018**, *73*, 143.
[8] B. Ozcelik, P. Pasic, P. Sangwan, C. L. Be, V. Glattauer, H. Thissen, R. A. Boulos, *ACS Omega* **2020**, *5*, 10288.
[9] H. Yuk, T. Zhang, S. Lin, G. A. Parada, X. Zhao, *Nat. Mater.* **2016**, *15*, 190.
[10] Z. Yang, Y. He, S. Liao, Y. Ma, X. Tao, Y. Wang, *Sci. Adv.* **2021**, *7*, abf9117.
[11] Y.-P. Li, W. Liu, Y.-H. Liu, Y. Ren, Z.-G. Wang, B. Zhao, S. Huang, J.-Z. Xu, Z.-M. Li, *Biomaterials* **2020**, *262*, 120336.
[12] B. Zhao, Y.-P. Li, Q. Wang, Y. Ren, Z.-L. Zheng, M.-H. Bai, J.-C. Lv, K. Li, J.-Z. Xu, Z.-M. Li, X. Song, *Chem. Eng. J.* **2022**, *427*, 130911.
[13] S. Ito, N. Shimohata, S. Iwanaga, W. Ito, M. Ohba, M. Mochizuki, T. Nakagawa, S. Suzuki, N. Sasaki, I. Koshima, U.-I. Chung, *Eur. J. Anaesthesiol.* **2012**, *29*, 100.
[14] M.-H. Bai, B. Zhao, Z.-Y.-T. Liu, Z.-L. Zheng, X. Wei, L. Li, K. Li, X. Song, J.-Z. Xu, Z.-M. Li, *Adv. Mater.* **2022**, *34*, 2108848.
[15] T. Crouzier, K. Boettcher, A. R. Geonnotti, N. L. Kavanaugh, J. B. Hirsch, K. Ribbeck, O. Lieleg, *Adv. Mater. Interfaces* **2015**, *2*, 1500308.
[16] B. Winkeljann, M. G. Bauer, M. Marczynski, T. Rauh, S. A. Sieber, O. Lieleg, *Adv. Mater. Interfaces* **2020**, *7*, 1902069.
[17] J. Song, T. M. Lutz, N. Lang, O. Lieleg, *Adv. Healthcare Mater.* **2021**, *10*, 2000831.
[18] S. Jahn, J. Klein, *Macromolecules* **2015**, *48*, 5059.
[19] B. Winkeljann, P. A. Leipold, O. Lieleg, *Adv. Mater. Interfaces* **2019**, *6*, 1900366.
[20] C. A. Rickert, B. Wittmann, R. Fromme, O. Lieleg, *ACS Appl. Mater. Interfaces* **2020**, *12*, 28024.
[21] G. D. Bixler, B. Bhushan, *Philos. Trans. R. Soc., A* **2012**, *370*, 2381.
[22] A. J. Scardino, in *Advances in marine antifouling coatings and technologies* (Eds: C. Hellio, D. Yebra), Woodhead, CRC, Oxford, Boca Raton **2009**, pp. 664–692.
[23] E. Ralston, G. Swain, *Bioinspiration Biomimetics* **2009**, *4*, 015007.
[24] E. S. Frenkel, K. Ribbeck, *Appl. Environ. Microbiol.* **2015**, *81*, 332.
[25] G. M. Bruinsma, H. C. Van Der Mei, H. J. Busscher, *Biomaterials* **2001**, *22*, 3217.
[26] L. Shi, R. Ardehali, K. D. Caldwell, P. Valint, *Colloids Surf., B* **2000**, *17*, 229.
[27] J. Y. Co, T. Crouzier, K. Ribbeck, *Adv. Mater. Interfaces* **2015**, *2*, 1500179.
[28] C. A. Rickert, M. G. Bauer, J. C. Hoffmeister, O. Lieleg, *Adv. Mater. Interfaces* **2022**, *9*, 2101716.
[29] S. Grumbein, M. Werb, M. Opitz, O. Lieleg, *J. Rheol.* **2016**, *60*, 1085.
[30] M. Marczynski, K. Jiang, M. Blakeley, V. Srivastava, F. Vilaplana, T. Crouzier, O. Lieleg, *Biomacromolecules* **2021**, *22*, 1600.
[31] B. Robertson, *Clin. Physiol.* **1983**, *3*, 97.
[32] J. Johansson, M. Some, B.-M. Linderholm, A. Almlen, T. Curstedt, B. Robertson, *J. Appl. Physiol.* **2003**, *95*, 2055.
[33] S. Tatur, A. Badia, *Langmuir* **2012**, *28*, 628.
[34] M. J. Bishop, E. A. Weymuller, B. R. Fink, *Anesth. Analg.* **1984**, *63*, 335.
[35] S. H. Baron, H. W. Kohlmoos, *Anesth. Analg.* **1975**, *54*, 767.
[36] J. Carlson, J. Mayrose, R. Krause, D. Jehle, *Ann. Emerg. Med.* **2007**, *50*, 686.
[37] N. Fernández-Bautista, J. A. Domínguez-Núñez, M. M. Castellano Moreno, M. Berrocal-Lobo, *Bio. Protoc.* **2016**, *6*, 2078.
[38] E. Mulaosmanovic, T. U. T. Lindblom, M. Bengtsson, S. T. Windstam, L. Mogren, S. Marttila, B. W. Alsanius, *Plant Methods* **2020**, *16*, 62.
[39] C. J. Cooksey, *Biotech. Histochem.* **2014**, *89*, 564.